Widening the Range of Trackable Environmental and Health Pollutants for Li#Garnet#Based Sensors

Widening the Range of Trackable Environmental and Health Pollutants

for Li-Garnet-Based Sensors

Moran Balaish[a] and Jennifer L.M. Rupp[a,b,*]

[a]Department of Materials Science and Engineering, Massachusetts Institute of Technology, 77 Massachusetts Avenue, Cambridge, MA 02139, USA

[b]Department of Electrical Engineering and Computer Science, Massachusetts Institute of Technology, 77 Massachusetts Avenue, Cambridge, MA 02139, US

[*]Corresponding author email: jrupp@mit.edu

Abstract

Classic chemical sensors integrated in phones, vehicles, and industrial plants monitor the levels of humidity or carbonaceous/oxygen species to track environmental changes. Current projections for the next two decades indicate the strong need to increase the ability of sensors to sense a wider range of chemicals for future electronics not only to continue monitoring environmental changes but also to ensure the health and safety of humans. To achieve this goal, more chemical sensing principles and hardware must be developed. Here, we provide a proof-of-principle for the specific electrochemistry, material selection, and design of a Li-garnet $Li_7La_3Zr_2O_{12}$ (LLZO)-based electrochemical sensor, targeting the highly corrosive environmental pollutant sulfur dioxide (SO_2). This work extends the prime use of LLZO as a battery component as well as the range of so far trackable pollutants for potential future sensor-noses. Novel composite sensing electrode designs using LLZO based on porous scaffold, employed to define a high number of reaction sites, allowed to successfully track SO_2 at the dangerous levels of 0–10 ppm with close-to-theoretical SO_2 sensitivity. The insights on the sensing electrochemistry, reactions involved and control over the interface sensing electrode/Li^+ electrolyte structures and phase stability provide first guidelines for future Li-garnet sensors to monitor with fast response a wider range of environmental pollutants and toxins.

This is the author manuscript accepted for publication and has undergone full peer review but has not been through the copyediting, typesetting, pagination and proofreading process, which may lead to differences between this version and the Version of Record. Please cite this article as doi: 10.1002/adma.202100314.

1 Introduction

1.1 Poor air quality: a threat to health and climate

According to the World Health Organization (WHO), outdoor and household air pollution kill an estimated seven million people every year, accounting for one in eight deaths worldwide.[1] Ozone layer depletion (fluorocarbons, halocarbons), acid rain (SO_x, NO_x, HCl), toxicity (SO_x, CO, NO_x), and global warming (raising CO_2, CH_4, fluorocarbon, O_3 levels) are caused by numerous chemical pollutants emitted from diverse natural and industrial processes.[2,3] In the U.S., these contributors have led to an increased occurrence of natural disasters such as wild fires and hurricanes, which will continue to result in vast environmental climate-change-driven migration and resettling. As a consequence, disparities in terms of quality of life for humans will become much larger, demanding an affordable infrastructure that can locally measure changes in air pollution and minimize climate-change-induced socio-economic conflicts. Shifts in the local temperature, humidity, and pollutant levels can lead to new diseases and their spread, which in turn requires a careful understanding and measurement of the interplay between these processes. With roughly 91% of the world's population living in urban areas breathing polluted air,[1] *solid-state sensors* at relatively low cost for the monitoring and control of environmental quality are imperative to preserve air quality, human health, and the environment. In this context, sulfur oxides, SO_2 and SO_3, make up a sizeable portion of harmful pollutants, which are emitted from residential, manufacturing, and construction sectors through the combustion

of sulfur-containing compounds in fossil fuels during oil and gas production and from natural processes such as volcanic eruptions and forest fires (**Figure 1a**).[4] Sulfur oxides may interact with the environment to cause toxicity, diseases, and environmental decay, playing a significant role in acid rain and having an adverse impact on forests, water, soil, corrosion, and human health (**Figure 1b**). [5–8] Moreover, considerable evidence indicates a link between SO_2 exposure and risk of missed abortion in the first trimester of pregnancy, alongside higher likelihood of stillbirth and birth defects due to maternal long-term exposure to pollutants. [9,10] The permissible exposure limit to SO_2 in the air and workplaces is 0.1–10 and 5 ppm, respectively, setting the upper limit for exposure without detrimental effects.[11,12] Conventionally, SO_2 concentrations are measured using one of two optical tracking technologies, IR spectroscopy, or UV absorbance spectroscopy, which are accurate and stable but rather expensive and dependent on bulky instruments (~ 50,000 cm^3) and thus not suitable for real-time continuous monitoring required in miniaturized applications (**Figure 1c**). Alternative detection methods include gas chromatography and flame emission spectrometry, which are expensive, time consuming, and demand high power and are thus impractical for real-time monitoring and feedback control on a daily basis.[11,13]

1.2 Finding room to improve SO_2 monitoring

In the quest to achieve continuous monitoring of harmful pollutants, solid-state resistive gas sensors employing semiconducting metal oxides (SMOX) have seen the widest spread in gas-sensing applications owing to their compactness and versatility.[14–16] The combination of their specific characteristics (*e.g.,* physical, chemical, electrical, and thermal stability as well as corrosion resistance) alongside low thin-film processing costs for the integration of micro-

array sensors for multiple gas detection has positioned metal oxides as the most advantageous materials for use in chemical sensors for applications in exhausts (500–1000 °C) or environmental monitoring (150–400 °C). For sensing of gaseous SO_2, SMOX is typically composed of functional ceramics such as ZnO, CeO_2, SnO_2, Ga_2O_3, WO_3, TiO_2, or In_2O_3, which interact and exchange electrons with the targeted gas, yielding a change in the resistance of the metal oxide.[17–20] Resistive SMOX sensors can detect low gas concentrations with a fast response (typically around seconds), yet their selectivity is generally poor and unsatisfactory for practical applications. This poor selectivity stems from the operation of SMOX sensors being fully based on changes in electrical resistance present rather than unspecific descriptors considering the possible adsorption of multiple gases.

The alternative to resistive sensing is to consider electrochemical gas sensors operating under thermodynamic equilibrium for the detection of CO_2, SO_2, and NO_x. Such sensors employ ion-conducting solid electrolytes, where the conductivity stems from mobile ions rather than electrons, reducing susceptibility to corrosion and increasing selectivity, especially at low operation temperatures.[21]

1.3 Solid-state electrochemical gas sensors

In a solid-state electrochemical gas sensor, a chemical gas species reacts at the electrode/ion-conductor interface where electrical charges are exchanged, resulting in an electrical signal that is directly related to the concentration or partial pressure of the gas species. Sensors for which the output is an electromotive force (emf) are referred to as potentiometric sensors (or impedancemetric/amperometric sensors if the output is electrical current) and can be used to track a wide variety of gaseous species. In other words, potentiometric solid-state electrochemical SO_2 sensors offer a promising alternative

to the inconvenient UV and IR methods (with large power demands, cost, and size) by simply measuring chemical quantities and transducing them into electrical signals that correspond to the concentration of a particular chemical species. Until now, the potentiometric configuration has been the most widely used owing to its simple structure and operation principle, avoiding the need for complex electronics and thus providing higher cost efficiency for a wide range of applications. The solid-state potentiometric gas sensors were classified by Weppner into three types, [22] where the ion species derived from the tracked gas coincide with either the mobile ion (type I), the immobile ion (type II), or neither the mobile nor immobile ion but, rather, other ion species through the auxiliary sensing electrode (type III). Compared to types I and II, type III potentiometric sensors allow the detection of complex gas species (CO_2, NO_2, SO_2) through the use of an auxiliary sensing electrode and a fast-ion-conducting electrolyte, obviating the need for separate gas environments for the sensing electrode (SE) and reference electrode (RE) (**Figure 2a**). The inherent simplicity of the structure of type III solid-state potentiometric electrochemical gas sensors, which are commonly constructed by combining a solid ion-conductor electrolyte with an auxiliary sensing electrode and a reference electrode, in addition to the direct voltage readout and scope for miniaturization have positioned them as an attractive detection method for various gases.[23] The emf of the cell is determined by the chemical potentials established at the sensing (μ_{Li}^{SE}) and reference electrodes (μ_{Li}^{RE}). At thermodynamic equilibrium, the measured voltage across the cell (E) is related to the partial pressure of the detected gas ($p(SO_2)^{SE}$) according to the Nernst equation (**Figure 2a**). The most widely used solid-state electrolytes in electrochemical gas sensors are O^{2-}-ion conductors including yttria-stabilized zirconia, [24] tungsten-stabilized bismuth oxide,

samarium-doped ceria, and Na^+-ion conductors such as sodium beta-alumina[25] and NASICON. [26] Nevertheless, the relatively low mobility of the ions (i.e. O^{2-}, Na^+) in the solid electrolyte remains a challenge for sensor operation. Typically, it necessitates rather high operating temperatures above 500 °C to ensure sufficient ionic conductivity for the solid electrolyte, which dictates the sensor's response and recovery time (**Figure 2b**).

1.4 State-of-the-art electrochemically tracking of SO_2

Most conventional solid electrolytes include either alkali-metal sulfates,[27,28] Ag-beta-Al_2O_3,[29] Na-beta-alumina Na_2O-Al_2O_3,[25] NASICON ($Na_3Zr_2Si_2PO_{12}$),[26] LISICON ($Li_{14}ZnGe_4O_{16}$),[30] or yttria-stabilized zirconia (YSZ).[24,31] Historically, the use of solid electrolytes for the detection of SO_2 and/or SO_3 was first suggested by Gauthier et al. in 1977.[32,33] As no solid electrolyte is based on the conduction of pure SO_4^{2-} ions, solid-state electrochemical SO_2 sensors are typically either type II based on sulfate-based solid electrolytes such as K_2SO_4, Na_2SO_4, Li_2SO_4, or Ag_2SO_4 or type III based on Na^+ conductors with an auxiliary sensing electrode, where a thermodynamic equilibrium persists between the solid electrolyte (ion conductor), current collector (electron conductor), and gas phase.[34] The first type III electrochemical solid-state SO_2 sensor, reported in 1985 by Maruyama *et al.*,[35] was based on a Na^+ ion conductor, namely NASICON, and a Na_2SO_4 auxiliary sensing electrode operated at 776 °C. Later on, to mitigate the instability of NASICON under the SO_2 environment at high temperatures, NASICON was replaced by a MgO-stabilized zirconia solid electrolyte and Li_2SO_4-$CaSO_4$-based auxiliary sensing electrode.[36] The sensor operated at 650 °C in the range of 2–200 ppm (>10 ppm SO_2 concentration step) with a response/recovery time of 8–15 s/6–8 min by combining an anion-conducting solid electrolyte (O^2) with a cation-conducting auxiliary sensing electrode

(Li^+), imposing the formation of an ionic bridge interphase layer at the anion–cation conductor heterojunction interface to achieve an electrochemical chain. More recently, Ma et al. reported a mixed-potential SO_2 gas sensor using a NASICON solid electrolyte and orthoferrite ($La_{0.5}Sm_{0.5}FeO_3$) as the sensing electrode and catalyst, respectively, to track sub-ppm levels of SO_2 (0.2–5 ppm) with a sensitivity of 86 mV/dec at 275 °C; however, data on response and recovery times stimulates follow-up work (**Figure 2b**).[37]

Practical commercial sensors for the detection of SO_x typically operate above 500 ºC and require relatively high power because of the following drawbacks: *i*) sluggish detection and regeneration of the sensor, originating from slow diffusion processes and insufficient oxygen-ion conductance in zirconia-based electrolytes (~10^{-8} S/cm at 300 °C) and poor ionic conductivity in NASICON (~10^{-7} S cm^{-1} at room temperature), resulting in limited speed of the electrode reaction and poor detection and/or response time (typically > ~5 min) of the sensor with even longer recovery times (not always available/reported)[30,38–41] and *ii)* low chemical stability of the electrolyte, causing unstable voltage response as well as poor reproducibility and long-term stability. Although research has been mainly focused on type III electrochemical sensors for SO_2 using a NASICON solid electrolyte with fair to good response, drawbacks associated with stability and transport issues require research attention.

1.5 Developing environmental sensors based on $Li_7La_3Zr_2O_{12}$ solid electrolyte

There has always been a strong tie between the material development of solid electrolytes for solid-state batteries (SSBs) and that for type III sensor applications, which is reviewed in more techno-historical detail in Ref. [[23]]. After their discovery, Li solid-state electrolytes were mostly first integrated in solid-state batteries, with their integration in sensors lagging

behind.[23] In some sense, the philosophy in the quest for an ideal ionic solid is the same, with stable and highest ionic conduction for either fast charging in the battery or fast sensor response being sought. Where the philosophy differs in is the sensing and stability requirement under much harsher gas and temperature environments. For instance, the Li-garnet $Li_7La_3Zr_2O_{12}$ (LLZO) is considered one of the promising solid electrolytes to be integrated in Li-metal-based SSBs considering its high room-temperature ionic conductivity (~mS cm^{-1} for the cubic phase), high chemical stability towards Li metal (reduction potential of 0.05 V vs. Li^+/Li), and wide electrochemical stability window. [42,43] Hence, it is not surprising that with the discovery of fast Li-garnet conductors as solid electrolytes for batteries, the idea for their integration in sensors to accelerate tracking of CO_2 soon followed.[44,45] Moreover, prior theoretical and experimental studies of LLZO stability towards humidity and CO_2 exposure[46,47] served as fertile ground for the development of LLZO-based sensors tracking CO_2. In 2018, $Li_{6.75}La_3Zr_{1.5}Ta_{0.25}O_{12}$ was newly employed as a Li electrolyte for a type III potentiometric electrochemical sensor, creating a potential between a gold reference electrode and Li_2CO_3 sensing electrode to track CO_2.[45] The sensors offered a fast response time of <60 s at the lowered operation temperature of ~320 °C, tracking 400–4000 ppm levels of CO_2.[45,48] These new sensing principles resulted in record-setting performance compared to that of state-of-the-art solid-state CO_2 sensors based on solid-state ionic conductors and led to new use cases of classic battery Li electrolytes for the sensing field.[23,48] Nonetheless, whereas some properties of fast-Li^+-conducting electrolytes may be more relevant for batteries, namely stability against Li metal, a wide electrochemical stability window, and favorable mechanical properties, solid-state electrochemical sensors require different requirements to operate well over the long

term and differ clearly towards the well-established solid state electrolyte materials in batteries, see Ref. [[43]] for detail. Primarily, investigation of the phase stability and transport properties upon prolonged exposure to the targeted gas and of the kinetic responses is needed. For instance, for battery operation in ambient conditions, a solid electrolyte may be targeted for 10^5 cycles and typical charge/discharge times of ~10 h, whereas an electrochemical sensor operates continuously (~days) and requires response times on the order of seconds in a reducing gas environment. One may also add here, that recent discussion on the adaptability and processability of known battery solid state battery electrolytes form bulk (pellet or tape form) to thin film form for which we refer to Ref. [[49]] has still to be translated to electrochemical gas sensors in future work as well. Given the potential to track CO_2, it is of high interest to expand the portfolio of LLZO-based sensors to also sense alternative pollutants; however, this possibility has not yet been explored. We see potential and express in this work that LLZO-based sensor hardware and its electrochemistry could be further developed for use in electronic noses, extending the range of trackable pollutants beyond CO_2, including new responses to corrosive SO_x environments and health threats.

This work provides a proof-of-principle for the electrochemistry, material selection, and design of SO_2 sensing for Li-garnet conductors and contributes to the field in two ways. From a broader view, this work demonstrates the ability of fast SSB Li conductors of the garnet group to serve additional functionalities beyond battery components, and their potential to serve as sensors not only for CO_2 but now also for SO_2 pollutants and health threats. Widening the spectrum of trackable pollutants to sulfur oxides and the intrinsically

fast response times resulting from the fast-conducting solid Li^+ electrolyte can serve as prerequisites for future sensor-nose technology and hardware in that area, which has not yet been expressed as an option. To succeed in proof-of-principle demonstration for SO_2 sensing, it is imperative to first probe the material stability in the rather corrosive environment of SO_2, which has not yet been studied for Li-garnet conductors because of their prime use case as electrolytes in batteries. In addition, there has never been a material selection and design proposal for electrodes and their microstructure to access the newly proposed SO_2 sensing electrochemistry, which we discuss and investigate in this work. Both are key to demonstrating whether such sensors can simply operate and to carefully discuss their characteristics in their response and recovery times and their sensitivity towards SO_2 concentration step changes and optimal operation temperature ranges. Collectively, these are the first steps to expand the applications of a classic battery electrolyte to serve additional purposes with adapted electrochemistry and cell design to sense an extended range of pollutants from CO_2 to SO_2 for future devices.

2 Results and Discussion

2.1 Defining the Chemical and Thermal Stability Window of $Li_7La_3Zr_2O_{12}$ for SO_2 Environments

Future SO_2 type III electrochemical sensors will require sufficient stability of the Li garnet electrolyte to maintain its phase and ensure sufficient Li conductivity to function for fast sensor response. To probe stability for the rather harsh environment, we fabricated dense and cubic Li-garnet solid-state electrolyte pellets ($Li_{6.5}La_3Zr_{1.5}Ta_{0.5}O_{12}$) via classic solid-state synthesis (see **Experimental** and **Supporting Information** for SEM, XRD, Raman, and

conductivity measurements of the unexposed pellets, **Figure S1**) and investigated their phase stability and microstructural changes when exposed to low and high SO_2 concentrations of 4–250 ppm at temperatures between 240 and 480 °C for 24 h. In the following, we discuss morphological changes observed using SEM (**Figure 3** and **S2**) and phase stability evaluated using both, XRD (**Figure S3)** and Raman spectroscopy (**Figure 4**)**,** to catch the potential changes in near-order vibration of the lattices in reaction to SO_2 exposure.

At low SO_2 concentrations (4 ppm), the cubic garnet structure was maintained over the entire probed temperature range, 25–480 °C. At temperatures of 320 °C and above, the XRD peak signature at 22.23° became more prominent, which corresponds to $(11\bar{1})$ diffraction of Li_2SO_4. We detected an increase in the thickness of the Li_2SO_4 layer formed on LLZO from 0.5 to ~2 µm upon increasing the temperature from 240 °C to 480 °C, according to the SEM cross sections, **Figure 3a** (see also **Figure S2**). For temperatures > 320 °C, a change in morphology from a continuous but porous layer of Li_2SO_4 to a non-continuous and dense island-like layer was observed (**Figure 3b**). Although the formation of Li_2SO_4 was likely enabled by the leaching of Li^+ ions (presumably) from the surface of the LLZO pellet followed by a reaction with SO_2 gas, its effect on the Li ionic conductivity of LLZO was found to be negligibly small, maintaining a conductivity of ~0.7 mS cm^{-1} at ambient, and the cubic structure prevailed (**Figure 4a** and **S4**) when electrochemical impedance spectroscopy was used to estimate the bulk ionic conductivity of the same LLZO pellet after 24-h exposure to 10 ppm of SO_2 at 240 and 480 °C (**Figure S4**). Moreover, XPS analysis of pristine LLZO pellet and after 24-h exposure to 10 ppm of SO_2 at 240 and 480 °C confirmed that sulfur was not incorporated in the LLZO structure and only as a surface layer (**Figure S5**).

At medium SO_2 concentrations (40 ppm), we observe at roughly the same temperature threshold of 320 °C the appearance of Li_2SO_4 in the SEM, XRD, and Raman analyses, which is consistent with the observation of low SO_2 concentration, **Figure 3a** and **S2**. The thickness of the Li_2SO_4 layer increased by one order of magnitude from ~350 nm at 240 °C to ~3.5 µm at 480 °C after exposure to 40 ppm SO_2. The top-view SEM micrographs (**Figure S2**) reveal more about the evolving growth of this layer starting from a porous morphology followed by an increase in grain size and densification of the Li_2SO_4 layer as a function of temperature (**Figure 3b**). The complete coverage of the LLZO pellet by the dense Li_2SO_4 layer aligns well with its principal observation in the Raman surface characterization (**Figure 4b**) and XRD bulk characterization (**Figure S3**). These results were accompanied by a color change of the pellet from yellowish to white > 400 °C.

At high SO_2 concentrations (250 ppm), we exposed the LLZO pellets to rather harsh conditions during a 24-h period and probed the effect of temperature between 240 and 480 °C. Up to the tested 40 ppm SO_2 exposure, we can confirm that the phase of the bulk LLZO did not change and remained cubic. At 250 ppm SO_2, XRD analysis (**Figure S3**) revealed that even though the prime cubic phase remained LLZO, there was pronounced Li loss and the formation of lanthanum zirconate ($La_2Zr_2O_7$), as indicated by the increasing intensity of the (111) diffraction peak at 28.5° with temperature (at both 240 and 480 °C). The cross-section (**Figure 3a**) and top-view (**Figure S2**) SEM micrographs reveal a continuous and dense Li_2SO_4 layer at 240 and 480 °C with thicknesses of ~2.5 and 4 µm, respectively, exclusively covering the surface of the LLZO pellet (see SEM micrographs, **Figure 3a**). Hence, we confirm that the cubic garnet structure was maintained as the majority phase up to 480 °C in the bulk; however, there is a threshold of ~240 °C where in very harsh SO_2 environments, Li leaches

out from the garnet LLZO structure notably in the process of forming the Li_2SO_4 surface layer (**Figure 4c**).

2.2 Conclusions on Optimal Processing and Operation Range for a Li-Garnet SO_2 Sensor

Exploring the spontaneous formation and morphological evolution of Li_2SO_4 under diverse SO_2 concentrations and temperatures suggests that the major auxiliary sensing electrode component should preferably be Li_2SO_4 to avoid its *in-situ* formation during sensor operation and to better manipulate its morphology and thickness through the formation of an artificial sensing electrode layer. The thermodynamic (**Supporting Information**) and kinetic tendency for the formation of Li_2SO_4 on LLZO at the investigated temperature and SO_2 concentration range was confirmed. The latter is of high importance, indicating the feasibility of SO_2 oxidation under the explored conditions, without the use of platinum (Pt) mesh (or other types of catalysts) typically employed to catalyze the oxidation of SO_2. [36] The investigation clarified that the SO_2 concentration should be kept to < 40 ppm, where the operation of the sensor at elevated temperatures (480 °C) could be realized without jeopardizing the cubic structure and high Li^+ conductivity of LLZO, considering the potential long-term operation of the sensor.

Next, we wish to consider that once an artificial Li_2SO_4 layer is introduced on top of the LLZO pellet as an auxiliary sensing electrode, the formation of a new Li_2SO_4 layer, formed *in situ* on top of the LLZO layer during sensor operation, may be kinetically inhibited. To confirm or refute the last assumption, additional stability investigation of garnet LLZO with an artificially deposited Li_2SO_4 layer was executed. Qualitative analysis conducted using SEM

micrographs and elemental mapping (**Figure S6**) of a LLZO pellet pre-deposited with Li_2SO_4 and exposed to 10 ppm SO_2 at 480 °C for 24 h revealed that the *in-situ* formation of the Li_2SO_4 layer was in fact inhibited. Thin (<500 nm) deposits (such as Li_2CO_3 and Li_2SO_4 deposits) were observed mainly at defected areas on the surface of the LLZO pellet. Moreover, as will be discussed in the following sections, post-mortem SEM and elemental mapping analysis of the sensing electrode/LLZO cross section revealed that the ~15–20-µm-thick sensing electrode remained unchanged throughout the sensing experiment (~24 h) without the appearance of a new deposit layer on top of the sensing electrode.

The phase and microstructure evolution indicate that the processing range to first establish the sensing electrode formation of Li_2SO_4 on LLZO are to be separated from the operation conditions of the sensor. *i.) Manufacture of the sensing electrode on LLZO pellets* is best served artificially in a pre-fabrication step to operation, where its microstructure and composition can be tuned efficiently. *ii.) Operation of the SO_2 sensor for LLZO* should proceed at a lower temperature and SO_2 level to keep the device steady and with low degradation. We conclude that the LLZO pellet remains primarily in the cubic phase, with no occurrence of the Li-loss phase observed for a critical amount of ~3 µm of Li_2SO_4 formed when operated later between 240 and 480 °C for 4–40 ppm SO_2. Considering that the regulation values for SO_2 detection in ambient atmosphere are 0.1–10 ppm and the stability analysis of Ta-doped $Li_7La_3Zr_2O_{12}$ under diverse SO_2 concentration and temperatures, the concentration of SO_2 in this study was determined to be 0–10 ppm SO_2, for which we can assure phase stability of the LLZO pellet to serve later as an electrolyte and stability of the

Li_2SO_4 after formation. Based on these results, we targeted a temperature range of 240–480 °C to evaluate to the SO_2 sensor performance and explore its effect on sensing.

2.3 Proof-of-Principle for Li-Garnet-Based SO_2 Sensors

As SO_2 sensors based on $Li_7La_3Zr_2O_{12}$ garnets do not yet exist, the electrochemical cell design and operational principles remain to be explored. In particular, the chemical stability of the sensing electrode/solid electrolyte requires careful analysis as the electrode/electrolyte interface plays a critical role in determining the performance characteristics of the gas sensor, which responds to the difference in the chemical potential of Li^+ at the interfaces of the electrode. Utilizing a Li-garnet LLZO solid electrolyte with an 'endless' Li^+-ion source of multiple cations that can easily diffuse to and from the auxiliary sensing electrode and chemically react either during the processing of the sensing electrode (750 °C) or during the operation of the sensor (480 °C) requires the exploration of the interplay between the auxiliary sensing electrode components and the Li-garnet solid electrolyte. It has been previously established that an auxiliary sensing electrode employing both Li_2SO_4 and $CaSO_4$ benefits from faster response time attributed to lower melting point and higher ionic conductivity of the two-component composite electrode.[38,50,51] In the particular material composite case of Li_2SO_4-$CaSO_4$|LLZO, both the sensing electrode and the solid electrolyte are Li^+-ion conductors; explicitly, Li^+ is the mobile ion. Thus, the electrochemical chain through the interface is simply achieved with Li^+ ions. This is in contrast to type III potentiometric electrochemical sensors, where the sensing electrode and solid electrolyte are based on different mobile ions (e.g., Li^+ conductor and O^{2-} conductor for Li_2SO_4|MSZ),[36] necessitating the formation of a mediating phase (ionic bridge) to provide a fast and stable electrochemical response by delivering a continuous path for ion conduction.[52–54]

Nonetheless, the formation of an interfacial layer at the sensing electrode/solid electrolyte interface provided by interdiffusion and chemical reactivity, accelerated during heat treatment during the sensing electrode coating process (750 °C) or operation of the sensor (480 °C), may occur and deteriorate the SO_2 sensing ability while establishing a complex voltage response due to competitive electrochemical reaction. Moreover, close inspection of the cross-sectional SEM micrographs and elemental mapping of a sensor after a prolonged sensing experiment (**Figure S7**) reveals an ~1–2-µm-thick Ca-rich layer sandwiched between the LLZO solid electrolyte and auxiliary sensing electrode.

To further investigate any possible chemical reaction between LLZO and the auxiliary sensing electrode (Li_2SO_4-$CaSO_4$) and identify any reaction products that may have been formed during high-temperature heat treatment, powder mixtures of LLZO and sulfates at different mole ratios were heated at 750 °C for 2 h in oxygen, and compositional analysis was performed using XRD (**Figure 5**). The results indicated that once $CaSO_4$ is exposed to heat treatment (either with or without Li_2SO_4), the decomposition product CaO is formed (followed by the evolution of O_2 and SO_2). Interestingly, for the $CaSO_4$ and LLZO mixture, the decomposition products included not only CaO but also Li_2SO_4 and $Ca_{0.7}La_{0.6}Zr_{0.7}O_3$ compounds, yet no indication of LLZO was evident. In other words, once $CaSO_4$ and LLZO were exposed to the typical heat treatment for a sensing electrode, the chemical reaction between the two components resulted in the complete consumption of the LLZO powder (or at least to the point where no LLZO was detected via XRD) and the formation of Li_2SO_4. To further corroborate the last finding, $CaSO_4$ paste was brushed on an LLZO pristine pellet and heat treated at 750 °C for 2 h in oxygen. XRD analysis (**Figure S8**) confirmed again the

presence of CaO, Li_2SO_4, and $CaSO_4$ as decomposition reaction products and validated the formation of Li_2SO_4 once a Li source (i.e. LLZO) and sulfate source (i.e. $CaSO_4$) are mixed together and heat treated. The results clarified that when using a Li-based solid electrolyte, although $CaSO_4$ still assured the melting of the sensing electrode at lower temperature, securing good adhesion between the sensing electrode and solid electrolyte, its role as a humidity absorbent may have been diminished. Once the Li_2SO_4 and LLZO mixture was heated, a decomposition product, possibly ZrO_2, was confirmed via XRD. However, the major decomposition products were evident once all three components, namely Li_2SO_4, $CaSO_4$, and LLZO, were mixed together, confirming the chemical instability between the garnet LLZO solid electrolyte and the sensing electrode Li_2SO_4-$CaSO_4$ during the heat-treatment procedure.

The lack of a stable interfacial compound or new decomposition products in the sensing electrode may account for the unstable behavior of the sensors and may require innovative auxiliary sensing electrode microstructure and composition design. Adding garnet LLZO to the auxiliary sensing electrode may further assist in both improving the ionic conductivity and response time of the sensor by *i)* creating percolation pathways, where clusters with improved Li^+-ion conductivity through the use of LLZO are randomly connected; *ii)* increasing the effective surface area reaction by creating triple-phase boundary (TPB) reaction zones while shortening the Li^+-ion diffusion distance from the auxiliary sensing to the garnet LLZO solid electrolyte; and *iii)* stabilizing the solid electrolyte itself by playing an active role in forming an interfacial layer, thus helping to achieve thermodynamic equilibrium. Two main processing strategies were undertaken in order to incorporate garnet

LLZO in the auxiliary phase (Li_2SO_4:$CaSO_4$): *i)* LLZO calcinated powder was directly added to the sensing electrode paste followed by heat treatment at 750 °C and *ii)* a porous LLZO scaffold was created by preparing a porous LLZO layer on top of the LLZO sintered pellet,[55] followed by infiltration of the sensing electrode paste and subsequent heat treatment at 750 °C (see **Experimental** section for detailed procedure).

Following this design, the SO_2 sensor was composed of the electrochemical cell expressed as

$$Au \mid Li_{6.54}La_{3.00}Zr_{1.36}Ta_{0.50}O_{11.73} \mid Li_2SO_4\text{-}CaSO_4\text{-}LLZO \mid Au, SO_2, O_2$$

, where gold (Au) is the reference electrode, $Li_{6.54}La_{3.00}Zr_{1.36}Ta_{0.50}O_{11.73}$ is the solid electrolyte, and Li_2SO_4–$CaSO_4$–LLZO is the composite sensing electrode. When the cell is heated to a stable thermal condition, mobile Li^+ ions in the sensing electrode and the solid electrolyte can effectively take part in the electrochemical reaction, shifting it to an equilibrium state.

At the auxiliary sensing electrode, the oxidation of SO_2 occurs according to the following reactions (**Figure 2a**):

$$[1]\ SO_2 + \frac{1}{2}O_2 \overset{K}{\leftrightarrow} SO_3\ ;\ [2]\ K = \frac{p[SO_3]}{p[SO_2]\cdot p[O_2]^{0.5}}$$

$$\Delta G_f^0 = -97{,}780 + 92.78T[\mathrm{K}],$$

, where K and ΔG_f^0 are the equilibrium constant and the standard Gibbs free energy change in both reactions, respectively [1]. Thermodynamically, the oxidation of SO_2 is feasible at room temperature and up to 780 °C. The overall reaction at the sensing electrode is expressed by,

$$[3]\ 2Li^+ + SO_3 + \frac{1}{2}O_2 + 2e^- \leftrightarrow Li_2SO_4.$$

At the reference electrode, Li^+ ions are expected to react mainly with oxygen and not sulfur dioxide, possibly according to the following equation:

$$[4]\ 2Li^+ + \frac{1}{2}O_2 + 2e^- \leftrightarrow Li_2O.$$

Considering that *i)* the temperature and the partial pressure of O_2 ($p[O_2]$) are fixed in our current measurement set-up (0.21 atm) and *ii)* the activity of Li_2SO_4 and Li_2O are kept constant and the concentration of Li^+ is assumed to remain unchanged through the measurement, the cell potential (emf), *E*, is only determined by the partial pressure of SO_2 ($p[SO_2]$) according to the Nernst equation:

$$[5]\ E = E^0 + \frac{RT}{2F}\ln(p[SO_2]),$$

, where E^0 is a constant (standard potential), *F* is the Faraday constant, *R* the gas constant, and *T* is the absolute temperature.

The electrochemical characterization of both devices to the SO_2 response is depicted in **Figure 6** and **7**. In the case of the incorporation of a porous LLZO scaffold as a part of the sensing electrode (**Figure 6a** and **6b**), a consistent increase in the emf of the sensor was observed in the electrochemical experiments measuring the emf response upon increase of SO_2 concentration steps (**Figure 6c**). The response time was determined to be ≥ ~30 min while the recovery time was achieved within ~4-15 min. Nonetheless, the sensitivity of the sensor was determined to be 20.34 mV/dec (*n*=7.3 e^-) and 8 mV/dec (*n*=18.6 e^-) for the sensor response step (0–10 ppm) and recovery step (10–0 ppm), respectively, significantly lower than the theoretical sensitivity for a two-electron reaction of 74.64 mV/dec (**Figure**

6d). The poor sensitivity may imply that the *in-situ* formation of Li_2SO_4 is not kinetically favorable at the new auxiliary sensing electrode, and thus, we turn next to the second alternative structure of the sensing electrode, that is, the composite sensing electrode. Once LLZO was added to the sensing electrode to create a dense composite electrode (**Figure 7a** and **7b**), the sensitivity of the sensor was determined to be 48.4 mV/dec (n=3.1 e^-) and 42.9 mV/dec (n=3.5 e^-) for the sensor response step (0–10 ppm) and recovery step (10–0 ppm), respectively (**Figure 7c** and **7d**). The response time of ≥ ~40 min and recovery time of ≥ ~24 min did not show improvement compared to those of the scaffold structure of LLZO (perhaps expected as a result of the less optimized network structure of the composite electrode); nevertheless, a complete recovery to the initial sensor voltage was achieved with similar sensitivity values upon increase and decrease of SO_2 concentration steps (**Figure 7d**). In the composite structure where LLZO was distributed more homogeneously between the sulfate components and chemically reacted with them, the auxiliary sensing electrode was able to achieve for the first time in this study a new and stable thermodynamic equilibrium through both the response and recovery steps. The emf response of the electrochemical cells depicted in **Figure 6a** and **7a** to SO_2 concentration step at lower temperatures such as 240, 360 and 400 ˚ C (not presented) did not show any meaningful response. Nonetheless, the most significant improvement in the response ability of the sensor was demonstrated for the composite sensing electrode by the operation of the sensor at significantly lower temperatures, namely 240 °C, which had not been achievable thus far for all the explored sensing electrode microstructures and compositions (**Figure 7e**). The response and recovery times of ≥ ~60 min and ≥ ~4 min, respectively, still require significant improvement, which may be achieved in the future by incorporating electronic

conductors in the composite sensing electrode to meaningfully increase the active reaction zones. The sensitivity value was determined to be 47.7 mV/dec (n=2.1 e^-) for the sensor response step (0–10 ppm), thus marking the auxiliary sensing electrode design as the first with a reported sensitivity value for the response reaction close to the theoretical value of 50.8 mV/dec (calculated for 240 °C) (**Figure 8**). It is hypothesized that lower operating temperature inhibits decomposition reactions between LLZO and Li_2SO_4–$CaSO_4$, ensuring a sensitivity close to the theoretical value, implying thermodynamic equilibrium when using a composite sensing electrode. However, the lower operating temperature evidently has a significant effect on the O_2/SO_2 desorption processes, decreasing the sensitivity to 8.2 mV/dec for the sensor recovery step (10–0 ppm), and may require the use of a catalyst to enable the operation of the sensor at such lower temperatures.

2.4 Perspective on SO_2 tracking and sensor design for Li-garnet LLZO

The successful design of an electrochemical potentiometric type III sensor tracking SO_2 necessitates the selection of materials in terms of chemistry and microstructure that provide a balance between an advantageous ion conductor, an auxiliary sensing electrode, and stable electrode/solid electrolyte interfaces, which play a critical role in determining the performance characteristics of the gas sensor. Most potentiometric type III SO_2 sensors, are either based on Na^+ conductors (NASICON), O^{2-} conductors (e.g., MgO, beta-alumina), Li^+ conductors (Li_3PO_4), or other alkaline-earth-ion-conducting electrolytes (e.g., $MgZr_4(PO_4)_6$) in pellet, tube, or thick-film form, typically operate at higher temperatures (500–800 °C) with a response time that varies from ~1 min to 20 min and characteristically longer recovery times (**Figure 2b**) when compared to the composite-sensing-electrode-based

sensor operated at 240 °C at close-to-theoretical sensitivities presented here (**Figure 8**).[23] Moreover, most reported sensors track SO_2 only in concentrations higher than 10 ppm towards hundreds and thousands of ppm of SO_2. Reported SO_2 sensors covering similar SO_2 concentration ranges tracked in this research typically operate at temperatures ≥ 500 °C, except for a thick-film SO_2 sensor based on NASICON solid electrolyte and $La_xSm_{1-x}FeO_3$ sensing electrode that has been reported to operate at 275 °C but only to detect sub-ppm levels of SO_2 (0.2–5 ppm).[37] Reported SO_2 sensors operating at lower temperatures (400–450 °C) have shown sensitivity values that correlate with the calculated theoretical values or divert by up to ~20%, with rather large spread in response times from ~18 s to 10 min.[56–58] In addition, most type III electrochemical sensors detecting SO_2 take advantage of the use of Pt (precious metal), V_2O_5 (toxic), or MgO (serves as a catalyst above 300 °C)[59] as a part of the auxiliary sensing electrode (or as an external addition to catalyze SO_2 oxidation) to effectively support fast SO_2 oxidation in addition to O_2/SO_2 adsorption and desorption processes and to significantly shorten the response/recovery time when the sensor is operated at lower temperatures. We wish to highlight that we have purposefully not taken advantage of any type of catalyst and focused on solely utilizing a fast ion conductor as a part of the sensing composite electrode and electrolyte to improve the diffusion process and reaction speed.

Indeed, Li-garnet LLZO has proven to show favorable thermodynamic and kinetic tendency for the formation of Li_2SO_4 over a wide temperature range, without hampering the bulk ionic conductivity of the LLZO pellet through prolonged exposure to SO_2. We conclude, that Li-garnet can serve as a potentiometric electrochemical sensor tracking SO_2 with a close-to-

theoretical sensitivity at a remarkably low operation temperature of 240 °C (**Figure 8**) through the introduction of a composite sensing electrode (Li_2SO_4–$CaSO_4$–LLZO). This sensing electrode design is expected to see wider success tracking other gases (e.g., CO_2) without requiring an additional catalyst for the oxidation/reduction of the parent gas. We see perspective to further improve the response time for practical application in follow up work, for which one may envision novel porous sensing electrode architectures, inspired by the solid-state-battery field.[60] Alternatively, by using composite sensing electrode designs that are frequently used for SSBs (but have seen less exploration in the solid-state-sensor field), guidelines for the development of sensor tracking SO_2 (and other types of chemicals) based on a LLZO solid electrolyte can be further developed, contingent upon the introduction of a catalyst to secure fast gas oxidation and adsorption/desorption processes at low operating temperature with significantly inhibited electrolyte degradation. In addition, we highlight the importance of exploring the sensing electrode designs in future work to not only other gases such as H_2O, H_2S, NH_3, and NO_X but also to explore the cross-sensitivity and sensor response to other gases and impurities while detecting SO_2.

3 Conclusion

Environmental sensors measuring a wide range of pollutants and toxins are essential in the early detection, real-time monitoring, systematic survey, analysis and simply for better management and safety of natural resources and humans. Particular interest is here to explore material classes and combinations thereof that may allow to measure not only a single pollutant but by a varied sensor electrode electrochemistry track a wide range of

pollutants (e.g., CO_2, SO_2, NO_2 and H_2S). The critical factors that determine the sensing performance for rather corrosive toxins such as SO_2 are to develop a suitable electrochemistry and sensor material selection stable in this environment, and operating at low temperature (ideally below 300 °C) to assure a low energy footprint per sensing device volume. One of the best investigated SO_2 electrochemical (type III) sensors are those based on the solid-state Na^+ conductor NASICON a known conductor vastly applied also as a battery solid state electrolyte. Despite the promise, the limited Na^+ conductivity at ambient around 10^{-7} S cm^{-1} challenges intrinsically to establish fast sensor response time and lower operation temperatures (energy footprint); which is also typically accompanied by degradation of the sensor performance and poor reproducibility. We propose in this work as a promising alternative cubic Li-garnet (LLZO) as a solid-state electrolyte for new SO_2 sensors due to their three orders of magnitude increased ionic conductivity (~mS cm^{-1}) and higher electrochemical stability window, which allows a wider definition and choice for sensing material electrodes. The material class of Li-garnets is known for about a decade[23,49] and has proven success for solid state batteries, however, it had only recently been introduced to serve as electrolyte for type III sensors tracking less corrosive gases such as CO_2 with fast sensing and recovery times.[44,45] Looking ahead to widen potentially the spectrum of species that the material class of Li-garnet conductors can track for future type III sensors or noses, we envisioned through this work to learn how stable these are in corrosive environments, whether these are suited to create sensor electrochemistry dedicated to SO_2 and answering the fundamental question whether the 0 to 10 ppm limit of SO_2 can be tracked with reasonable performances to be meaningful for future environmental monitoring and analysis.

Taking key stability factors into account, such as making sure that the phase of the Li-garnet and conductivity are unchanged during SO_2 exposure of up to 10 ppm at maximum temperature of 480 °C, we could define functioning sensing devices based on Li_2SO_4–$CaSO_4$–LLZO composite sensing electrodes and Li-garnet solid electrolyte (LLZO) and prove their performance. For that, we explore the following sensor electrochemistry $2Li^+ + SO_3 + \frac{1}{2}O_2 + 2e^- \leftrightarrow Li_2SO_4$ and investigated the major aspects that affect the electromotive force response according to the Nernstian behavior and the response/recovery time of the sensor, explicitly the auxiliary sensing electrode composition and microstructure. To assure a higher enough triple phase boundary, novel configurations, inspired by the battery field, were employed, namely composite designs of the auxiliary sensing electrode utilizing LLZO as a powder or porous scaffold. The SO_2-sensor operated at 480 °C with sensitivities ranging from 8 to 49 mV/dec and recovery/response times ranging from 4 to 60 min depending on the auxiliary sensing electrode configuration and SO_2 concentration. The introduction of the composite sensing electrode Li_2SO_4–$CaSO_4$–LLZO with the LLZO electrolyte conductor achieved close-to-theoretical sensitivity of 47.7 mV/dec at remarkably low operating temperature of the sensor of 240 °C. We wish to highlight that this outperforms previously reported SO_2 type III electrochemical sensors operating on Zr^{4+} (400 °C) or Na^+ (600 °C) ion-conducting solid electrolytes in terms of their operation temperature and has as a consequence impact on the sensor power consumption (**Figure 8**).

This work demonstrates the ability to widen the functionalities of Li-garnet solid electrolytes beyond batteries and expands the spectra of trackable pollutants even under harsh environmental conditions from CO_2 to now also SO_2. The material selection and design

proposed for the electrodes and their microstructure unlocked the newly proposed SO_2 sensing electrochemistry, which provides first guidelines for continuous, real-time monitoring of SO_2 in practical applications. We foresee that the high phase stability and wide electrochemical stability window of Li-garnet electrolytes may serves many Lithionic[23] applications beyond batteries and in particular for future electrochemical sensor architectures. We envision that besides the known trackable CO_2 pollutant, and now in this work added SO_2, also other pollutants such as NO_x, and H_2S may be suitable to be sensed with type III Li-garnet based electrochemical sensors in the future. Certainly, exploring the cross-sensitivity and sensor response to other gases, moisture and impurities while detecting SO_2 remains to be explored and offers new research areas. We look ahead to see according sensor electrode material design and electrochemistry to-be-developed.

4 Experimental Section

4.1 Synthesis of LLZO solid electrolyte

The solid electrolyte $Li_{6.5}La_3Zr_{1.5}Ta_{0.5}O_{12}$ was prepared via solid-state synthesis using stoichiometric amounts of $La(OH)_3$ (Sigma-Aldrich, 99.9%), ZrO_2 (Sigma-Aldrich, 99.9%), and Ta_2O_5 (Sigma-Aldrich, 99.99%) and an excess amount of 50 wt.% LiOH (Alfa Aesar, purity 99.8%) to compensate for the lithium evaporation during the sintering process. The precursors were mixed and homogenized by planetary milling (PM, Across International, PQ-N04) in absolute isopropanol using ZrO_2 balls for 1 h at 500 rpm and then dried at 90 °C. The obtained powder was packed in the form of pellets, placed in MgO crucibles, and first-calcinated at 750 °C for 10 h at a heating rate of 5 °C min^{-1} under the constant flow of synthetic air. Next, the powder was grinded and ball-milled in absolute isopropanol for

another 12 h and then dried at 90 °C. The dried powder was second-calcinated at 750 °C in air for 5 h at a heating rate of 10 °C min^{-1} under the constant flow of synthetic air. Finally, each ~0.5 g of the powder was pressed into a pellet using a die with a diameter of 12 mm and thickness of 1.5 mm in a uniaxial press (2.2 tons·cm^{-2}). The green pellets were sintered in a MgO crucible under a constant flow of pure oxygen (50 sccm) at 1100 °C for 5 h at heating/cooling rates of 10 °C min^{-1}. The sintered LLZO pellets were dry-polished to ensure consistency among all the samples. We disclose the chemical, thermal, and electrical characterization of the pristine LLZO pellets in detail in the **Supporting Information**.

4.2 Fabrication of the sensing electrode and sensor device

Auxiliary (sensing) electrode. The auxiliary electrode was prepared by mixing appropriate mole ratios of lithium sulfate (Li_2SO_4; anhydrous, 99.99% trace metal basis, BeanTown Chemical) and calcium sulfate ($CaSO_4$; anhydrous, 99.99% trace metal basis, BeanTown Chemical) with 10 wt.% of the synthesized LLZO powder. A binder solution (mixture of α-terpineol and ethylene cellulose) was added to the different (Li_2SO_4:$CaSO_4$):LLZO powder mixtures in a weight ratio of 1:2; the resulting mixture was crushed and homogenized using a mortar until a smooth paste was produced. The paste was brushed on a quarter of the solid electrolyte and heated at 750 °C for 2 h at a heating rate of 10 °C min^{-1} under the constant flow of pure oxygen (50 sccm). After the auxiliary (sensing) electrode preparation, a gold paste (Conductive Epoxy GOLD Paste, EMS) was brush-painted on the second quarter of the solid electrolyte surface, serving as the reference electrode (RE). A thin layer of the gold paste was brushed on the auxiliary (sensing) electrode, serving as a current collector. Platinum wires (0.1-mm diameter, 99.995%, BeanTown Chemical) were connected to the auxiliary (sensing) and reference electrodes using the gold paste. The complete sensor

construction was annealed at 300 °C for 4 h in an oxygen atmosphere to cure the gold paste. An adhesive sealant was applied on the reference electrode (898FS, Cotronics Corp.) and cured again at 300 °C for 2 h in an oxygen atmosphere.

\

Porous LLZO scaffold layer. Inspired by the recent designs taken from the solid-state-battery field,[55] a porous LLZO layer was prepared by brushing a paste of the sintered LLZO powder and binder solution (mixture of α-terpineol and ethylene cellulose) with a 1:1 weight ratio on top of the LLZO pellet. Corn starch (Sigma-Aldrich) was added as a pore former. The sample was sintered at 1100 °C for 2 h under oxygen flow. Once a porous LLZO scaffold was formed, a sensing electrode paste was sprayed on top of the porous LLZO and further heated to 750 °C for 2 h at a heating rate of 10 °C min^{-1} under the constant flow (50 sccm) of oxygen.

Spraying procedure of the sensing electrode. When better control of the thickness and geometry of the sensing electrode was required (for instance, in the case of the porous LLZO scaffold layer), a spraying procedure was employed. Appropriate amounts of the Li_2SO_4 and $CaSO_4$ powders were weighed and ball-milled in absolute isopropanol for another 3 h. The homogenized suspension was loaded into a spray gun (high-precision dual-action gravity feed airbrush, Gocheer) and sprayed on the LLZO pellet using a shadow mask. The sprayed sensing electrode was then heated at 750 °C for 2 h at a heating rate of 10 °C min^{-1} under the constant flow (50 sccm) of pure oxygen.

Chemical stability investigation of LLZO solid electrolyte and auxiliary sensing electrode components. Powder mixtures of LLZO and the sulfates, i.e., LLZO:Li_2SO_4:$CaSO_4$, in different mole ratios (namely 1:0:1, 1:1:2, 0:1:1, 1:0:0, 0:1:0, and 1:1:0) were thoroughly mixed using

a mortar and pestle, packed into a 12-mm diameter die, and heated at 750 °C for 2 h at a heating rate of 10 °C min^{-1} under the constant flow (50 sccm) of pure oxygen. The reaction products were identified using XRD.

4.3 Sensing system setup and electrochemical sensing measurements

The SO_2 gas sensing experiments were conducted and measured using a Linkam stage (HFS600E) with an internal volume of ~50 cm^3 equipped with a heating element in the temperature range of 25–600 °C. The experimental set-up consisted of two automated mass flow controllers (red-y, Vogtlin Instruments, Switzerland) for 50 ppm SO_2 balanced by dry synthetic air and dry synthetic air (20% O_2 in N_2). Reference humidity, ambient temperature, and SO_2 sensors (BW Clip SO_2 single gas detector, BW Technologies by Honeywell GasAlert Extreme Portable Sulfur Dioxide Monitor) were situated at the outlet of the measurement chamber. Different concentrations of the analyzed gas mixture, namely SO_2, flown over the sensing electrode while maintaining a constant oxygen concentration of 20 vol.%, were prepared by diluting 50 ppm of SO_2 balanced by synthetic air (20% O_2, 80% N_2) with dry synthetic air (20% O_2, 80% N_2) through a set of automated mass flow controllers (MFCs). The sensitivity of the sensor was evaluated through sensing experiments where the open-circuit voltage (OCV) was measured as a function of SO_2 concentration at a constant and calibrated temperature of either 240, 320, 400, or 480 °C at a heating/cooling rate of 10 °C min^{-1}. The temperature calibration of the sensor was performed on the surface of the garnet LLZO pellet. The SO_2 profile was held with 2.5-ppm steps applied for 1–2 h in the range of 0–10 or 1–15 ppm SO_2. The open-circuit voltage was measured using a Keithley 2612B electrometer. The reference and auxiliary (sensing) electrodes were contacted using the Pt wires, which were glued to the electrodes with gold paste.

4.4 Surface and bulk characterization (EIS, SEM/EDS, in-situ/ex-situ XRD, ICP, Raman)

Electrochemical impedance spectroscopy. The electrical properties of the garnet LLZO solid electrolyte were investigated using impedance spectroscopy (VSP-300 potentiostat/galvanostat, Bio-Logic, Knoxville, TN, USA). The applied frequency range was 7 MHz to 1 Hz with a 20-mV AC amplitude. The LLZO sintered pellet was double-sided dry polished and subsequently covered with 150-nm Au electrodes by DC sputtering. The sample was placed in an air-tight T-cell.

X-ray diffraction. XRD patterns of the solid electrolyte and the sensing electrodes were recorded using a Rigaku SmartLab diffractometer with Cu Kα irradiation (λ = 1.5406 Å). A step size of 0.01° and counting time of 3 s at 45 kV and 200 mA over the angular range of 10°–80° were used for the measurement.

Induced coupled plasma mass spectrometry. The Li, La, Zr, and Al atomic compositions were determined by ICP-MS spectroscopy (Agilent 7900 ICP-MS) with an orthogonal detector system (ODS), which allows a wide dynamic concentration detection range from sub-ppt to percent-level concentration. Prior to the analysis and to avoid incorrect readings due to the formation of Li_2CO_3 at the surface of the LLZO pellets, the samples were polished and a weighted amount was scraped off the sintered Ta-doped LLZO pellet and dissolved in aqua regia (36.5 wt.% HCl 99.999% and 65–70 vol% HNO_3 99.999%, trace metals basis, BeanTown Chemical) at 60 °C for 48 h in a closed vial to obtain clear solution. The solution was diluted immediately before the ICP-MS analysis. For internal standard purposes, 10 ppm Tb was used (10 ppm 3% v/v HNO_3, Ricca Chemical Company) and calibration standard solutions were prepared from 10 ppm in 2% HNO_3 Li, La, Zr, and Al standards (Ricca Chemical

Company) and diluted accordingly to prepare 0–10 ppm calibration standard solutions for each element. The ICP-MS results were normalized to the lanthanum and oxygen concentrations, estimated based on charge balance. The measurement was repeated at least 3 times.

Raman. The near-order characterization was performed using a confocal WITec alpha300 M+ Raman microscope (WITec, Germany) equipped with 532-nm excitation wavelength. All the Raman spectra were collected in ambient air.

Scanning electron microscopy. Field-emission scanning electron microscopes (FESEM Ultra Plus and FESEM Supra55VP equipped with an energy-dispersive X-ray spectrometer for elemental analysis and mapping, Zeiss) and a scanning electron microscope (SEM JEOL 7900F) equipped with a wide variety of detectors, including an EDS detector and a soft X-ray emission spectrometer (SXES) detector, allowed the efficient and parallel collection of very low-energy rays with chemical state analysis. The different scanning electron microscopes were employed to characterize the microstructure of the pristine LLZO pellets and complete sensor assemblies in addition to their post-mortem analysis after exposure to SO_2 at elevated temperatures.

Supporting Information

Supporting Information is available XXX.

Author Contributions

M.B and J.L.M.R proposed the LLZO-based SO_2 sensor concept. M.B proposed the sensor design, performed the experiments, and analyzed the results. M.B and J.L.M.R wrote the manuscript.

Conflicts of interest

The authors declare no conflicts of interest.

Acknowledgments

This work was supported in part by SENSE.nano under award number 2629303. M.B. acknowledges financial support from the US-Israel Fulbright Program, the Zuckerman Israeli Postdoctoral Scholar Program, and the MIT-Technion Postdoctoral Fellowship. J.L.M.R. thanks the Thomas Lord Foundation for financial support. This work made use of the MRSEC Shared Experimental Facilities at MIT, supported by the National Science Foundation under award number DMR-1419807. This work was performed in part at the Center for Nanoscale Systems (CNS), a member of the National Nanotechnology Coordinated Infrastructure Network (NNCI), supported by the National Science Foundation under NSF award no. 1541959. CNS is part of Harvard University.

References

[1] World Health Organization (WHO), "Ambient air pollution - a major threat to health and climate," can be found under https://www.who.int/airpollution/ambient/en/, **n.d.**

[2] J. Hansen, M. Sato, P. Kharecha, G. Russell, D. W. Lea, M. Siddall, *Philos. Trans. R. Soc. A Math. Phys. Eng. Sci.* **2007**, *365*, 1925.

[3] C. P. Chen, S. K. Tiong, S. P. Koh, F. Y. C. Albert, F. K. M. Yapandi, in *2018 3rd Int. Conf. Smart Sustain. Technol.*, **2018**, pp. 1–7.

[4] L. M. Sunil Dahiya, Andreas Anhäuser, Aidan Farrow, Hubert Thieriot, Avinash Chanchal, *Ranking the World's Sulfur Dioxide (SO2) Hotspots: 2019-2020 A Closer Look at the Colourless Gas That Is Poisoning Our Air and Health*, **2020**.

[5] M. Kermani, S. Fallah Jokandan, M. Aghaei, F. Bahrami Asl, S. Karimzadeh, M. Dowlati, *Heal. Scope* **2016**, *5*.

[6] Y. Wu, R. Li, L. Cui, Y. Meng, H. Cheng, H. Fu, *Chemosphere* **2020**, *241*, 125031.

[7] G. Goudarzi, S. Geravandi, E. Idani, S. A. Hosseini, M. M. Baneshi, A. R. Yari, M. Vosoughi, S. Dobaradaran, S. Shirali, M. B. Marzooni, A. Ghomeishi, N. Alavi, S. S. Alavi, M. J. Mohammadi, *Environ. Sci. Pollut. Res.* **2016**, *23*, 22001.

[8] N. Greenberg, R. S. Carel, E. Derazne, A. Tiktinsky, D. Tzur, B. A. Portnov, *J. Toxicol. Environ. Heal. Part A* **2017**, *80*, 326.

[9] L. Zhang, W. Liu, K. Hou, J. Lin, C. Zhou, X. Tong, Z. Wang, Y. Wang, Y. Jiang, Z. Wang, Y. Zheng, Y. Lan, S. Liu, *Nat. Sustain.* **2019**, *2*, 1011.

[10] S. Ha, D. Ph, R. Sundaram, D. Ph, M. B. Louis, D. Ph, C. Nobles, D. Ph, *Fertil. Steril.* **2018**, *109*, 148.

[11] D. D. Lee, *IEEE Sens. J.* **2001**, *1*, 214.

[12] Centers for Disease Control and Prevention (DCD), "NIOSH Pocket Guide to Chemical Hazards - Sulfur dioxide," can be found under https://www.cdc.gov/niosh/npg/npgd0575.html, **2019**.

[13] Y. Liu, J. Parisi, X. Sun, Y. Lei, *J. Mater. Chem. A* **2014**, *2*, 9919.

[14] G. Korotcenkov, *Mater. Sci. Eng. B* **2007**, *139*, 1.

[15] M. K. Ram, *Sensors for Chemical and Bioligocal Applications*, CRC Press/Taylor And Francis, **2010**.

[16] K. Kalantar-zadeh, *Sensors: An Intoductory Course*, Springer Science+Business Media New York, **2013**.

[17] H. M. E.B.Va´rhegyi, J.Gerblinger, F.Re´ti, I.V.Perczel, *Sensors Actuators B Chem.* **1995**, *25*, 631.

[18] D. Girardin, F. Berger, A. Chambaudet, R. Planade, *Sensors Actuators B Chem.* **1997**, *43*, 147.

[19] F. Berger, M. Fromm, A. Chambaudet, R. Planade, *Sensors Actuators B Chem.* **1997**, *45*, 175.

[20] Y. Shimizu, N. Matsunaga, T. Hyodo, M. Egashira, *Sensors Actuators B Chem.* **2001**, *77*, 35.

[21] N. Miura, S. Yao, Y. Shimizu, N. Yamazoe, *Sensors Actuators B. Chem.* **1992**, *9*, 165.

[22] W. Weppner, *Sensors and Actuators* **1987**, *12*, 107.

[23] J. L. M. Zhu, Y; Gonzalez-Rosillo, J C; Balaish, M; Hood, Z D; Kim, K J; Rupp, *Nat. Rev. Mater.* **2020**, DOI https://doi.org/10.1038/s41578-020-00261-0.

[24] Y. Yan, Y. Shimizu, N. Miura, N. Yamazoe, *Chem. Lett.* **1992**, *21*, 635.

[25] R. Akila, K. T. Jacob, *Sensors and Actuators* **1989**, *16*, 311.

[26] S.-D. Choi, W.-Y. Chung, D.-D. Lee, *Sensors Actuators B Chem.* **1996**, *36*, 263.

[27] N. Imanaka, Y. Yamaguchi, G. Adachi, J. Shiokawa, *J. Electrochem. Soc.* **1987**, *134*, 725.

[28] G. Adachi, N. Imanaka, *Chem. Sens. Technol.* **1991**, *3*, 131.

[29] P. H. Yang, J. H. Yang, D. K. Peng, G. Y. Meng, *Soild State Ionics* **1996**, *86*, 1095.

[30] G. Jasinski, P. Jasinski, B. Chachulski, A. Nowakowski, *J. Eur. Ceram. Soc.* **2005**, *25*, 2969.

[31] F. Liu, Y. Y. Wang, B. Wang, X. Yang, Q. Wang, X. Liang, P. Sun, X. Chuai, Y. Y. Wang, G. Lu, *Sensors Actuators, B Chem.* **2017**, *238*, 1024.

[32] M. Gauthier, A. Chamberland, A. Belanger, M. Poirier, *J. Electrochem. Soc.* **1977**, *124*, 1584.

[33] M. Gauthier, A. Chamberland, *Solid-State Detect.* **1977**, *124*, 1579.

[34] G. Korotcenkov, *Handbook of Gas Sensor Materials*, **2014**.

[35] T. Maruyama, Y. Saito, Y. Matsumoto, Y. Yano, *Solid State Ionics* **1985**, *17*, 281.

[36] Y. Yan, Y. Shimizu, N. Miura, N. Yamazoe, *Sensors Actuators B* **1994**, *20*, 81.

[37] C. Ma, X. Hao, X. Yang, X. Liang, F. Liu, T. Liu, C. Yang, H. Zhu, G. Lu, *Sensors Actuators B Chem.* **2018**, *256*, 648.

[38] F. Ménil, B. O. Daddah, P. Tardy, H. Debéda, C. Lucat, *Sensors Actuators B Chem.* **2005**, *107*, 695.

[39] G. Jasinski, P. Jasinski, B. Chachulski, A. Nowakowski, *Mater. Sci.* **2006**, *24*.

[40] H. Wang, Z. Liu, D. Chen, Z. Jiang, *Rev. Sci. Instrum.* **2015**, *86*, 75007.

[41] H. Wang, D. Chen, M. Zhang, J. Wang, *Surf. Coatings Technol.* **2017**, *320*, 542.

[42] R. Mahbub, K. Huang, Z. Jensen, Z. D. Hood, J. L. M. Rupp, E. A. Olivetti, *Electrochem. commun.* **2020**, *121*, 106860.

[43] K. J. Kim, M. Balaish, M. Wadaguchi, L. Kong, J. L. M. Rupp, *Adv. Energy Mater.* **2020**, 2002689.

[44] Y. Zhu, V. Thangadurai, W. Weppner, *Sensors Actuators, B Chem.* **2013**, *176*, 284.

[45] M. Struzik, I. Garbayo, R. Pfenninger, J. L. M. Rupp, *Adv. Mater.* **2018**, *30*, 1.

[46] L. Cheng, E. J. Crumlin, W. Chen, R. Qiao, H. Hou, S. Franz Lux, V. Zorba, R. Russo, R. Kostecki, Z. Liu, K. Persson, W. Yang, J. Cabana, T. Richardson, G. Chen, M. Doeff, *Phys. Chem. Chem. Phys.* **2014**, *16*, 18294.

[47] A. Sharafi, S. Yu, M. Naguib, M. Lee, C. Ma, H. M. Meyer, J. Nanda, M. Chi, D. J. Siegel, J. Sakamoto, *J. Mater. Chem. A* **2017**, *5*, 13475.

[48] C.-M. Horejs, *Nat. Rev. Mater.* **2018**, *3*, 41578.

[49] M. Balaish, J. C. Gonzalez-Rosillo, K. J. Kim, Y. Zhu, J. D. Hood, J. L. M. Rupp, *Nat. Energy* **2021**, DOI 10.1038/s41560-020-00759-5.

[50] A. Lundén, K. Schroeder, H. Ljungmark, *Solid State Ionics* **1988**, *28–30*, 262.

[51] K. Singh, V. K. Deshpande, *Solid State Ionics* **1984**, *13*, 157.

[52] N. Ma, S. Ide, K. Suematsu, K. Watanabe, K. Shimanoe, *ACS Appl. Mater. Interfaces* **2020**, *12*, 21515.

[53] T. Kida, H. Kawate, K. Shimanoe, N. Miura, N. Yamazoe, *Solid State Ionics* **2000**, *136–137*, 647.

[54] and N. Y. Y. Yan, N. Miura, Y. Yan, N. Miura, N. Yamazoe1, *J. Electrochem. Soc.* **1996**, *143*, 609.

[55] K. J. Kim, J. L. M. Rupp, *Energy Environ. Sci.* **2020**, *13*, 4930.

[56] Y. Uneme, S. Tamura, N. Imanaka, *J. Sensors Sens. Syst.* **2012**, *1*, 29.

[57] K. Chen, M. Zhang, H. Wang, H. Gu, *Rev. Sci. Instrum.* **2019**, *90*, DOI 10.1063/1.5080474.

[58] N. Rao, C. M. van den Bleek, J. Schoonman, O. T. Sørensen, *Solid State Ionics* **1992**, *53–56*, 30.

[59] J. H. Lunsford, *J. Catal.* **1972**, *26*, 261.

[60] G. T. Hitz, D. W. McOwen, L. Zhang, Z. Ma, Z. Fu, Y. Wen, Y. Gong, J. Dai, T. R. Hamann, L. Hu, E. D. Wachsman, *Mater. Today* **2019**, *22*, 50.

[61] B. K. Min, S. D. Choi, *Sensors Actuators, B Chem.* **2003**, *93*, 209.

[62] N. Izu, G. Hagen, D. Schönauer, U. Röder-Roith, R. Moos, *J. Ceram. Soc. Japan* **2011**, *119*, 687.

[63] X. Liang, T. Zhong, B. Quan, B. Wang, H. Guan, *Sensors Actuators B Chem.* **2008**, *134*, 25.

[64] R. Akila, K. Jacob, *J. Appl. Electrochem.* **1988**, *18*, 245.

[65] S. Suganuma, M. Watanabe, T. Kobayashi, S. I. Wakabayashi, *Solid State Ionics* **1999**, *126*, 175.

[66] and M. G. Jianhua, Yang, Yang Pinghua, *Sensors Actuators B* **1996**, *31*, 209.

[67] L. Wang, R. V. Kumar, *Mater. Res. Bull.* **2005**, *40*, 1802.

[68] M. Itoh, E. Sugimoto, Z. Kozuka, *Trans. Japan Inst. Met.* **1984**, *25*, 504.

[69] L. Wang, R. V. Kumar, *J. Appl. Electrochem.* **2006**, *36*, 173.

[70] L. Wang, R. V. Kumar, *J. Electroanal. Chem.* **2003**, *543*, 109.

Figures

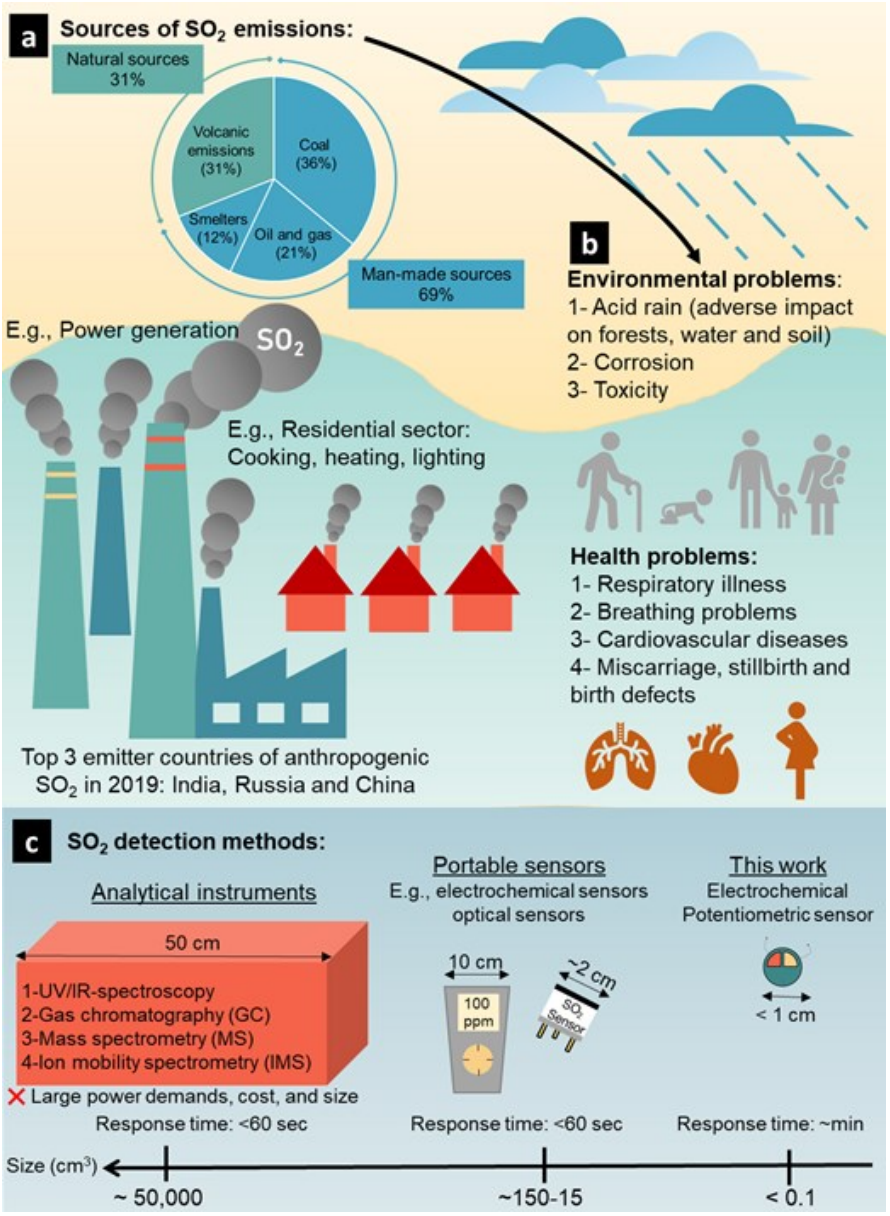

Figure 1. Schematic illustration of (a) natural and industrial sources of SO_2 emissions,[4] (b) environmental and health problems associated with the emission of SO_2 polluters, and (c) current detection methods of SO_2 gas.

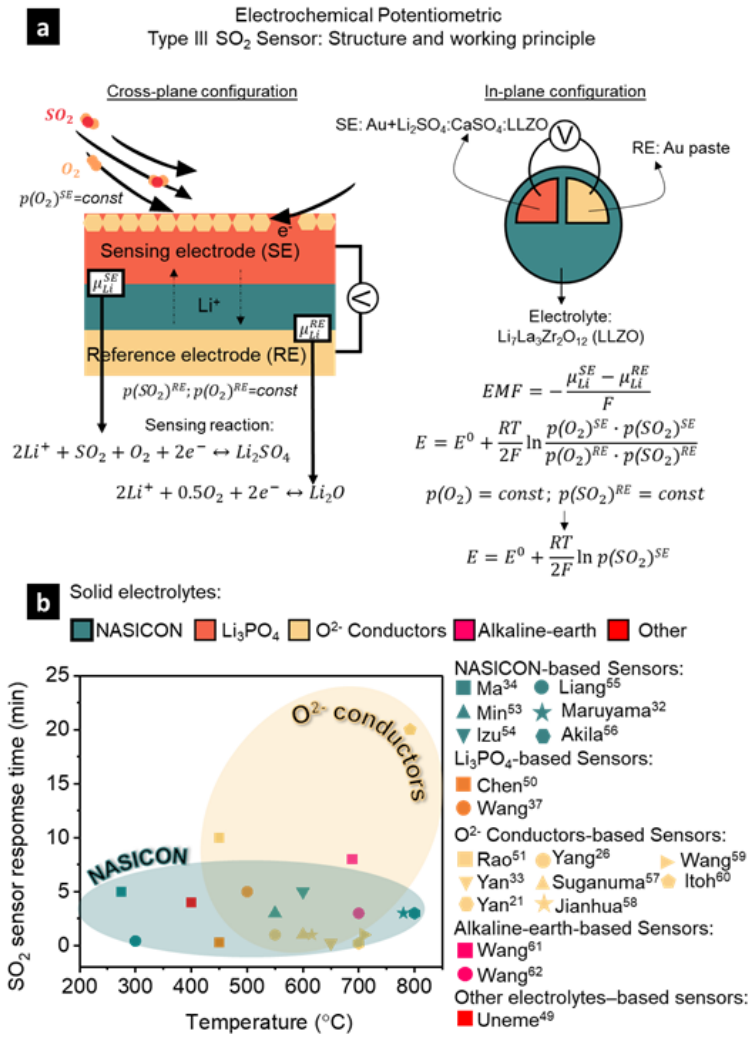

Figure 2. (a) Sensing principles of type III potentiometric sensor tracking SO_2 based on Li^+-based solid electrolyte, auxiliary sensing electrode, and gold (Au) reference electrode. The chemical gas species SO_2 reacts at the electrode/ion conductor interface, where electric charges are exchanged, resulting in an electric signal that is directly related to the concentration or partial pressure of the gas species according to the Nernst equation. EMF is the electromotive force of the cell, μ_{Li+} is the chemical potential of Li^+ at the sensing electrode or reference electrode, and *F* is the Faraday constant. (b) Response time of SO_2 potentiometric type III sensors based on typical solid electrolytes as a function of the operating temperature based on literature information. [Ma[37], Min [61], Izu[62], Liang[63], Maruyama[35], Akila[64]; Chen[57], Wang[40]; Rao[58], Yan[36], Yan[24], Yang[29], Suganuma[65], Jianhua[66], Wang[67], Itoh[68]; Wang[69], Wang[70]; Uneme[56]].

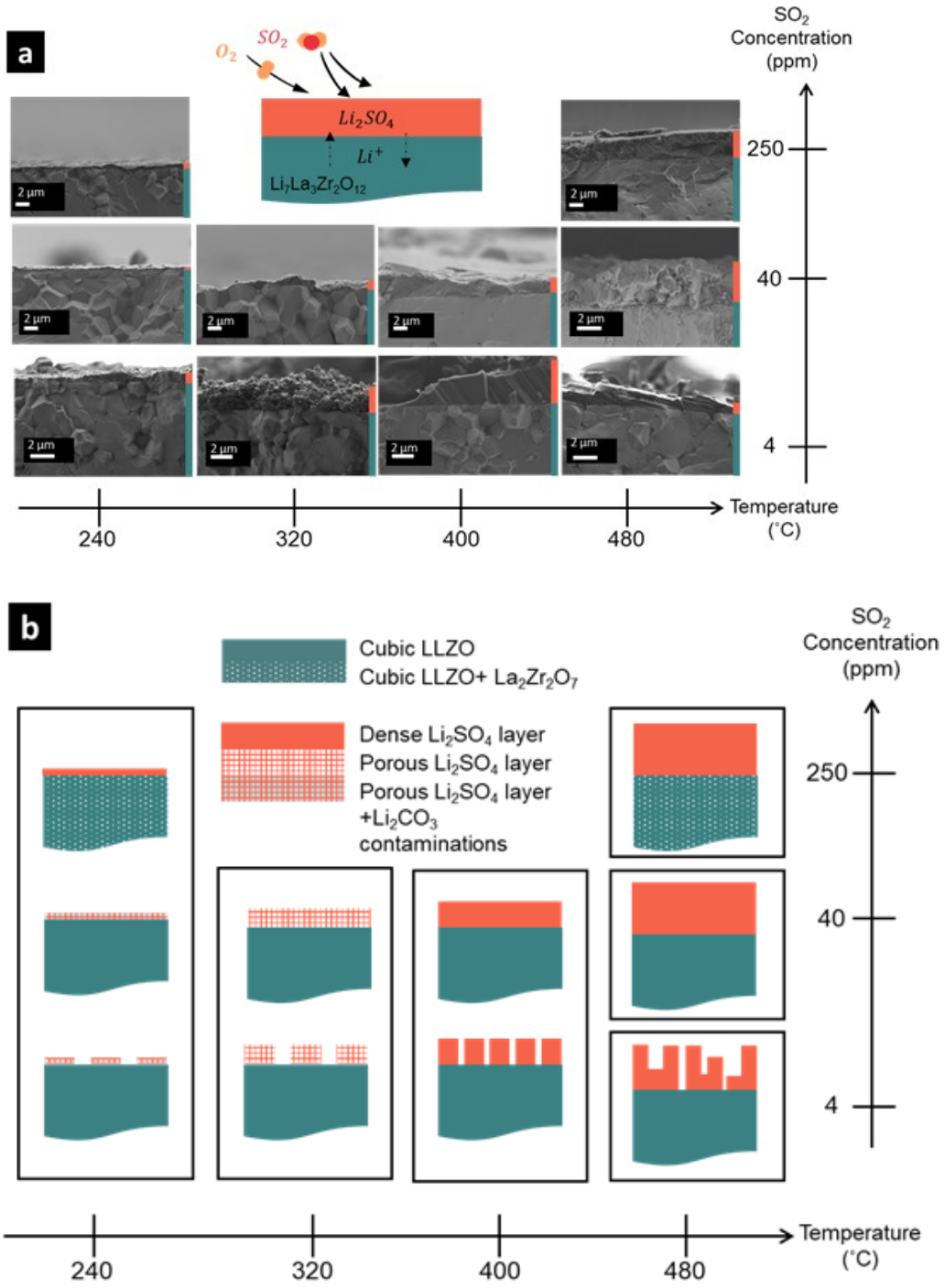

Figure 3. (a) Cross-sectional SEM micrographs of LLZO pellets after exposure to 4, 40, and 250 ppm SO_2 at 240, 320, 400, and 480 °C for 24 h. The formation of Li_2SO_4 was observed in all the studied cases. (b) XRD (and Raman) characterization of the surface of the LLZO pellets after exposure to 4, 40, and 250 ppm SO_2 at 240, 320, 400, and 480 °C for 24 h. In all the cases, Li_2SO_4 was confirmed to be the main component of the surface layer and LLZO maintained its cubic phase. At high SO_2 concentration (250 ppm), the formation of $La_2Zr_2O_7$ was observed.

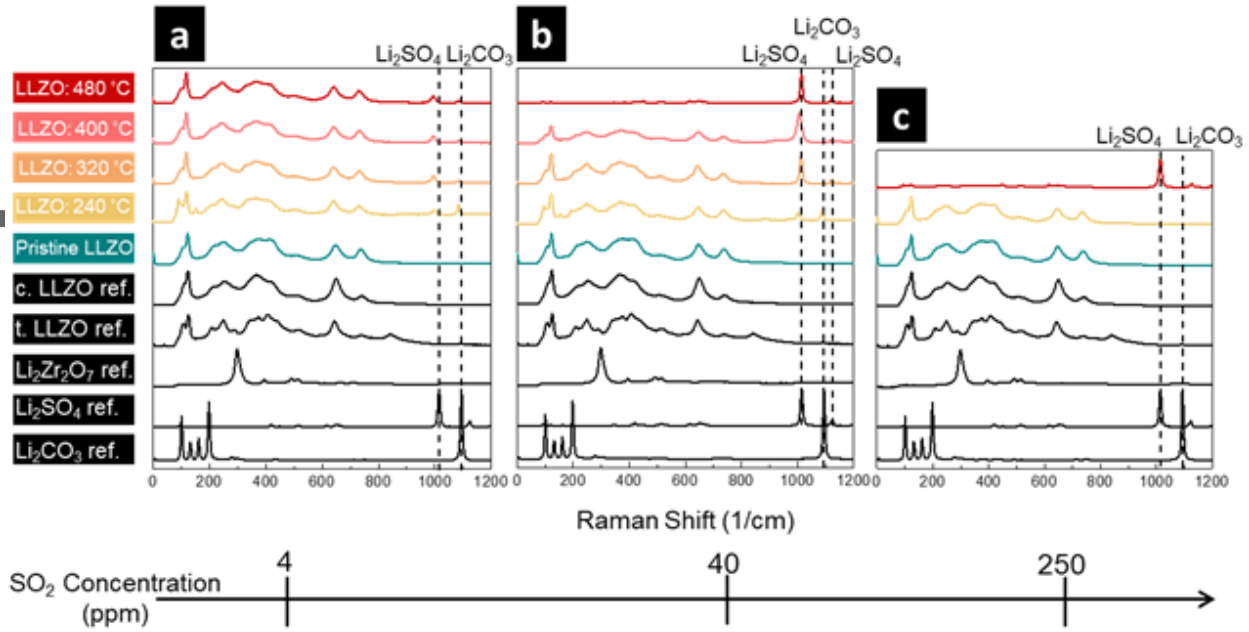

Figure 4. Raman spectra of LLZO pellets before (dark cyan) and after exposed to (a) 4, (b) 40 and (c) 250 ppm of SO_2 at 240 (yellow), 320 (orange), 400 (pink) and 480 ˚C (red) for 24 h. In all cases Li_2SO_4 was confirmed as the main component of the surface layer while LLZO maintained its cubic phase. At high SO_2 concentration (250 ppm), the formation of $La_2Zr_2O_7$ was observed. Additional reference spectra of Li_2CO_3, Li_2SO_4, $Li_2Zr_2O_7$, t. LLZO (tetragonal $Li_{6.5}La_3Ta_{0.25}Zr_{1.5}O_{12}$) and c. LLZO (cubic $Li_{6.5}La_3Ta_{0.25}Zr_{1.5}O_{12}$) are also displayed in black.

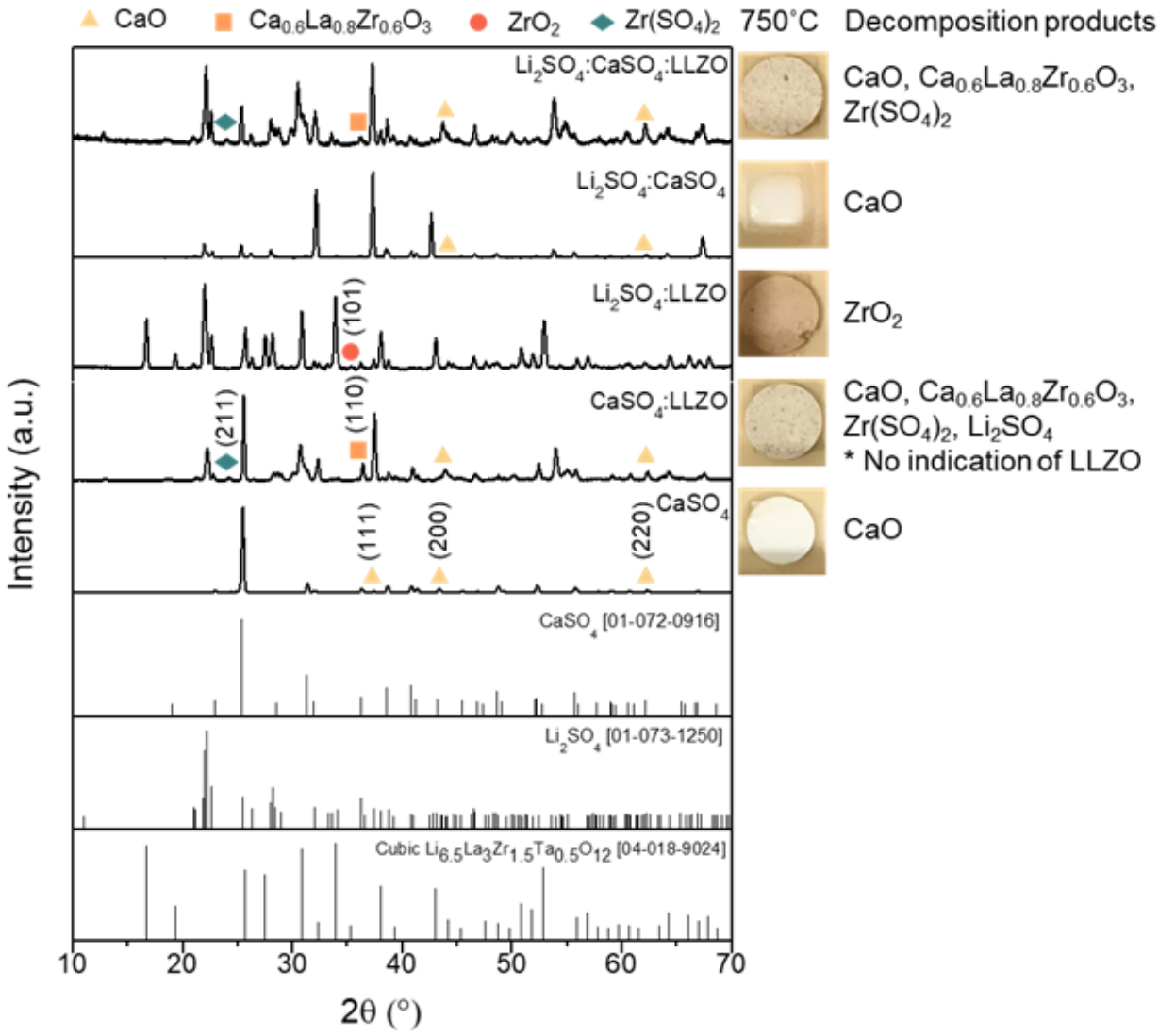

Figure 5. Chemical composition study of $CaSO_4$, Li_2SO_4, and LLZO powders after they were compacted into model pellets and heat-treated at 750 °C for 2 h in oxygen. Once $CaSO_4$ is exposed to elevated temperatures, the decomposition product CaO is formed. Once a mixture of $CaSO_4$ and LLZO powders was exposed to 750 °C, Li_2SO_4 was observed with no indication of LLZO. CaO [04-007-9734]; ZrO_2 [01-070-7358]; $Ca_{0.6}La_{0.8}Zr_{0.6}O_3$ [01-075-0354]; $Zr(SO_4)_2$ [00-024-1499].

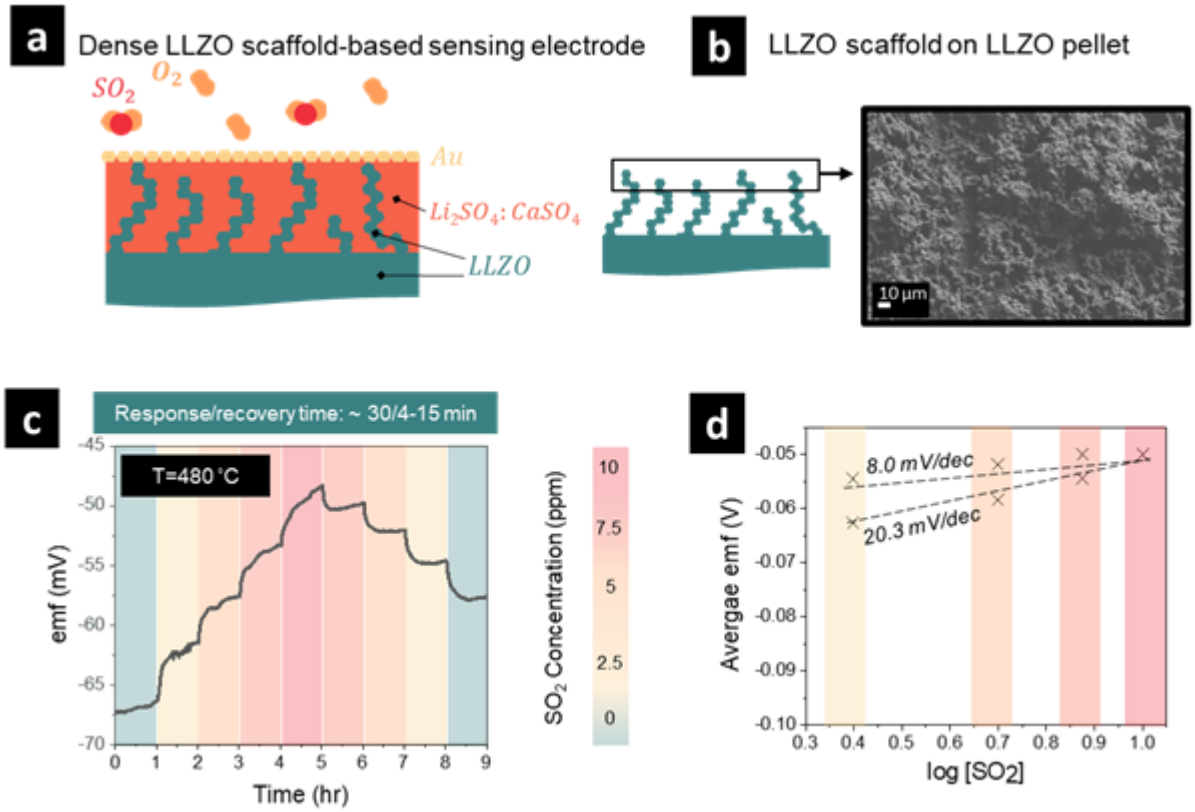

Figure 6. (a) Schematic illustration of SO_2 sensor with a LLZO-scaffold-based sensing electrode with a dense microstructure. (b) Top-view SEM micrographs of the LLZO scaffold on top of the LLZO pellet. (c) Emf response to SO_2 concentration step change (0–10 ppm) at 480 °C of the dense, LLZO-scaffold-based sensing electrode (recovery/response times are stated above and were extracted from the graphs). (d) Emf dependence on the SO_2 concentration on logarithmic scale showing sensitivity for dense, LLZO auxiliary sensing electrode.

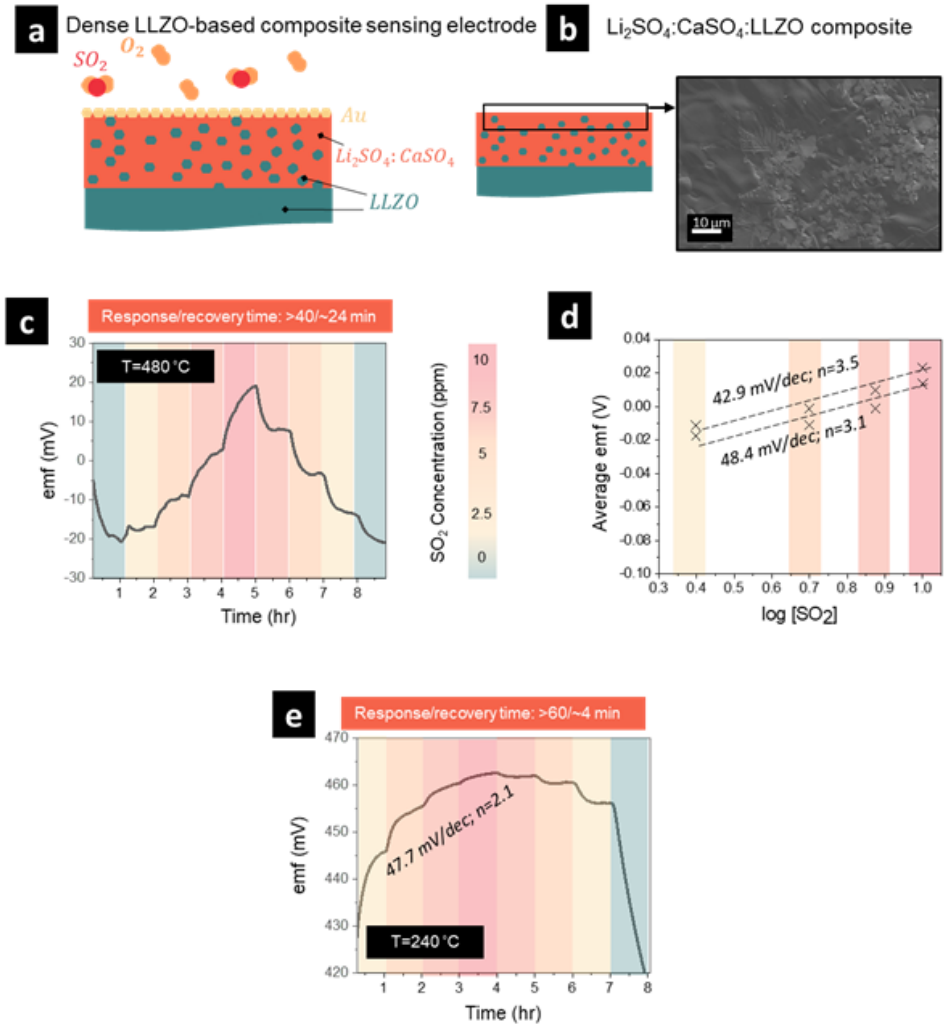

Figure 7. (a) Schematic illustration of SO_2 sensor with a dense LLZO-based composite sensing electrode microstructure. (b) Top-view SEM micrographs of the dense LLZO-based composite sensing electrode. (c) Emf response to SO_2 concentration step change (0–10 ppm) at 480 °C of the sensor (recovery/response times are stated above and were extracted from the graphs). (d) Emf dependence on the SO_2 concentration on logarithmic scale showing sensitivity for the dense LLZO-based composite sensing electrode auxiliary sensing electrodes. (e) Emf response to SO_2 concentration step change (0–10 ppm) at 240 °C of the dense LLZO-based composite sensing electrode (recovery/response times are stated above and were extracted from the graphs).

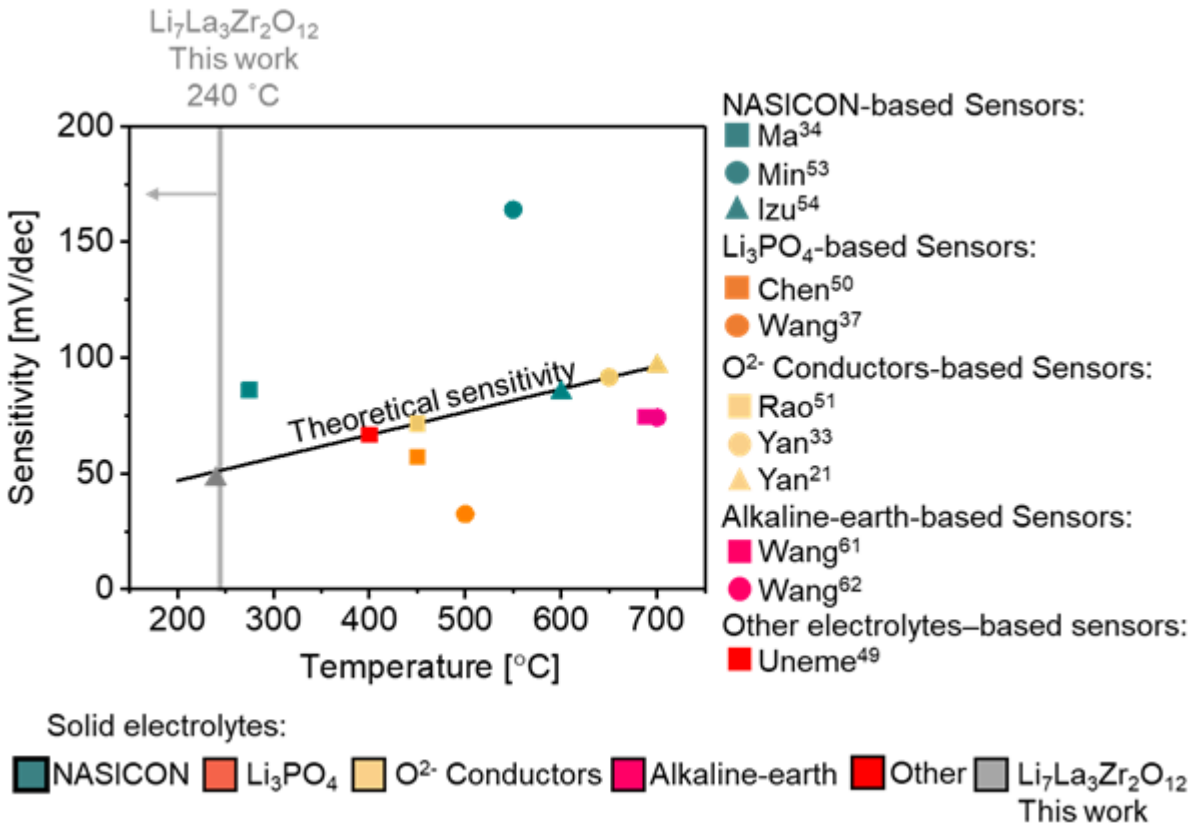

Figure 8. Comparison of the sensitivity (mV/dec) of SO_2 potentiometric sensors based on different solid-electrolyte types as a function of their operating temperature (°C).

ToC

The electrochemistry, material selection, and design of a Li-garnet $Li_7La_3Zr_2O_{12}$ (LLZO)-based electrochemical sensor, targeting the highly corrosive environmental pollutant sulfur-dioxide (SO_2) is presented. The insights on the sensing electrochemistry, reactions involved and control over the interface sensing electrode/Li^+ electrolyte structures and phase stability provide first guidelines for future Li-garnet sensors to monitor with fast response a wider range of environmental pollutants.